Quantum Dressed Classical Mechanics: Application to the HO + CO → H + CO_2 Reaction

Karen L. Feilberg, Gert D. Billing,* and Matthew S. Johnson

Department of Chemistry, H.C. Ørsted Institute, University of Copenhagen, DK-2100 Ø Copenhagen, Denmark

Received: August 17, 2001; In Final Form: October 11, 2001

Reaction dynamics of a four atom system (HO + CO) is investigated using the classical trajectory method and two quantum-classical theories. At 298 K, the new quantum-classical method predicts a rate of 1.49×10^{-13} cm^3/s, compared to an experimental value of 1.5×10^{-13} cm^3/s. It also reproduces the unusual temperature dependence.

1. Introduction

The utilization of quantum-classical methods for the treatment of molecular dynamics problems, in particular for *N*-body systems (with $N > 3$), for which a full quantal approach is numerically cumbersome, is extremely attractive because it attempts to incorporate the most important quantum effects into a framework which maintains the classical simplicity, both conceptual and computational, connected to the integration of the equations of motion. Recently, the quantum theory has been reformulated in such a manner that these mixed quantum-classical theories emerge naturally from a certain parametrization of the time-dependent Schrödinger equation.[1−9] Here, we use the theory to study the reaction between HO and CO.

The reaction of carbon monoxide (CO) with the hydroxyl radical (OH) is the final stage in the oxidation of carbon-containing compounds by combustion and through atmospheric photochemistry. This reaction is the principle source of heat in hydrocarbon flames and, in the atmosphere, the principal sink of both OH and CO. Accordingly, the reaction has received a great deal of attention from theorists[10−13] and experimentalists[14] and is the focus of several reviews.[15,16,25] The system is unusual for a bimolecular reaction as the rate constant is relatively insensitive to temperature; increases with pressure; and shows large H/D, C, and O isotope effects.[15−20] The high-pressure limit of the reaction rate has not been observed. These observations are consistent with an indirect mechanism. The reaction coordinate is complex, involving a saddle point on the entrance and exit channels (TS1 and TS2) and an intermediate barrier (TS3). TS1 involves the conversion of the initial hydrogen-bound complex OH−CO to the intermediate carboxyl radical species (HOCO).[21] There is a large barrier (TS2) for the hydrogen atom to leave the system. In addition, there is a small barrier within the intermediate, for the interconversion of *cis*- and *trans*-HOCO.[13]

Previous theoretical investigations have ranged from quantum reduced dimensionality (and $J = 0$) studies[22] over quantum-classical calculations[23] to quasiclassical trajectory studies.[24] The reaction is, in the present paper, studied theoretically using two different quantum-classical theories as well as the so-called quasiclassical trajectory method. The results are compared with available experimental data.

2. Theory

The Hamiltonian for a system of two diatoms in a space-fixed Jacobi coordinate frame, where, for the case investigated here, r_1 and r_2 are the vectors of the CO and OH bonds, respectively, and **R** is the vector connecting the centers of mass of the two molecules, can be written as

$$H = \frac{1}{2\mu}(P_X^2 + P_Y^2 + P_Z^2) + \sum_{i=1,2}\frac{1}{2m_i}(p_{x_i}^2 + p_{y_i}^2 + p_{z_i}^2) + V_{\mathrm{int}}(\{\mathbf{R}_{ij}(i \neq j)\}) + V_{\mathrm{M}}(r_1) + V_{\mathrm{M}}(r_2) \quad (1)$$

where the reduced masses are defined as

$$m_1 = m_C m_O/(m_C + m_O) \quad (2)$$

$$m_2 = m_O m_H/(m_O + m_H) \quad (3)$$

$$\mu = \frac{(m_C + m_O)(m_O + m_H)}{(m_C + 2m_O + m_H)} \quad (4)$$

and the momentum vector for the relative motion is (P_X, P_Y, P_Z) and for the two molecules (p_{x_i}, p_{y_i}, p_{z_i}) ($i = 1,2$). The intermolecular potential can be expressed in terms of six variables as for instance the atom−atom distances $\mathbf{R}_{ij}$ ($i \neq j$). For the isolated system, we introduce two Morse potentials V_M. The above Hamiltonian can now be used for classical trajectory studies of the chemical reaction by solving the 18 coupled equations of motion along trajectories, which are initialized for molecules in a specific vibrational/rotational state.[26] The problem with a classical treatment of reactions has to do with mainly two aspects, namely, tunneling and conservation of zero-point vibrational energy. Both of these problems can be handled by treating the motion in the r_1 and r_2 bonds quantally. The question is then how this quantization should be introduced. In some of our previous work,[9,27] we have solved the classical dynamics of the remaining degrees of freedom, i.e., all degrees of freedom except r_1 and r_2 in an effective mean field potential over the quantum variables. Another possibility (which is also used in this paper) is to solve the classical dynamical equations as in ordinary trajectory calculations, i.e., in the full space, and the quantum dynamics using the time-dependent Schrödinger equation (TDSE) in r_1 and r_2 space, i.e.

$$i\hbar\frac{\partial\Psi(r_1, r_2, t)}{\partial t} = \hat{H}_q\Psi(r_1, r_2, t) \quad (5)$$

where

10.1021/jp013206a CCC: $20.00
Published on Web 11/20/2001

$$\hat{H} = -\sum_i \left[\frac{\hbar^2}{2m_i}\frac{\partial^2}{\partial r_i^2} + V_M(r_i)\right] + V_{int}(r_1, r_2, t) \qquad (6)$$

where the time-dependence of the potential arises from the dependence of classical variables. We have also used this method in the present paper. The results are denoted "2D quantum-classical", but we emphasize that although this procedure looks physically sound it is ad hoc.

If we wish to solve the classical dynamics in its *full* dimensionality for a given system, what then are the quantum mechanical equations which consistently go along with that solution? This important question has recently found its solution by the time-dependent Gauss−Hermite discrete variable representation (TDGH-DVR) method as formulated in refs 1−9. Below, we shall briefly repeat the main features of this new dynamical theory.

2.1. TDGH-DVR Formulation. In the TDGH-DVR method,[6] the wave function for the system, which in Jacobi coordinates will be of dimension 9, is expanded in the Gauss−Hermite basis set.[1] If this expansion is inserted in the TDSE, we generate the classical equations of motion for the nine degrees of freedom. Aside from these equations of motion, we obtain a large matrix equation in the Gauss−Hermite basis representation. Instead of solving these, we can switch to a discrete variable representation (DVR). This procedure yields a set of equations, now involving the amplitudes for the specific DVR points. The DVR is by construction defined to follow the classical trajectories in space. Furthermore one grid point in a given dimension corresponds to a classical treatment of it. With many grid points we approach the quantum limit. The idea then in the present calculations is to use one grid point in all degrees of freedom except r_1 and r_2. For the spectator bond $r_1 = r_{CO}$ we can use a modest number of points,[9] whereas the bond which breaks requires more DVR points for a proper description. Because one grid point corresponds to a classical treatment, we shall illustrate the derivation by considering just the two degrees of freedom treated with more than one grid point, i.e., instead of giving the derivation in nine dimensions, we give it in two. However, we emphasize that the final equations are those which would come out of a nine-dimensional formulation assuming then afterward only one grid point in seven of the dimensions!

Thus, the wave function $\Psi(r_1, r_2, t)$ is first expanded in the Gauss−Hermite basis set as

$$\Psi(r_1, r_2, t) = \sum_{n_1,n_2} a_{n_1,n_2}(t)\Phi_{n_1}(r_1, t)\Phi_{n_2}(r_2, t)\phi_{n_1}(r_1, t)\phi_{n_2}(r_2, t) \qquad (7)$$

where $\Phi_{n_k}(r_k, t)$ is

$$\Phi_{n_k}(r_k, t) = \pi^{1/4}\exp\left(\frac{i}{\hbar}(\gamma_k(t) + p_k(t)(r_k - r_k(t)) + Re\, A_k(t)(r_k - r_k(t))^2)\right) \qquad (8)$$

with $k = 1$ and 2 and

$$\phi_{n_k}(\xi_k, t) = \frac{1}{\sqrt{n_k!2^{n_k}\sqrt{\pi}}}H_{n_k}(\xi_k)\exp\left(-\frac{1}{2}\xi_k^2\right) \qquad (9)$$

where $H_{nk}(\xi_k)$ is an Hermite polynomial and

$$\xi_k = \sqrt{2\,\mathrm{Im}\,A_k(t)/\hbar}(r_k - r_k(t)) \qquad (10)$$

Thus, $r_k(t)$ is the center of the wave packet in r_k, which, in its ground state, i.e., when $n_k = 0$, is a Gaussian wave packet. The basis set is also characterized by a momentum parameter $p_k(t)$, by a width parameter $A_k(t)$, and by a phase $\gamma_k(t)$.

N_1 and N_2 are the highest index of the Hermite polynomials used in r_1 and r_2, respectively, and thus, they represent the number of grid points in each quantum degree of freedom in the DVR approach. In this way the grid points in the kth degree of freedom are determined by the number of zeroes of the N_kth Hermite polynomial, and their position is not fixed in time, but it varies as a function of the time dependent variables Im $A_k(t)$ and $r_k(t)$, being

$$r_{k,i} = r_k(t) + \sqrt{\frac{\hbar}{2\,\mathrm{Im}\,A_k(t)}}z_i; \quad k = 1 \text{ and } 2 \qquad (11)$$

for the i−th grid point, where z_i is the i-th zero of the Hermite polynomial of order N_k.

To introduce the DVR representation, we use the following relation:

$$a_{n_1n_2}(t) = \sum_{ij} c_{n_1n_2}(t)\phi_{n_1}(z_i)\phi_{n_2}(z_j) \qquad (12)$$

where z_i are grid points of the Hermite polynomial, i.e., $H_{N_k}(z_i) = 0$. The DVR basis functions are orthorgonal:[4−6]

$$\int dr_1\, dr_2\, \psi_{ij}(r_1, r_2, t)\psi_{lm}(r_1, r_2, t) = \delta_{i,l}\delta_{j,m}S_1S_2 \qquad (13)$$

where S_k is defined as

$$\sum_{n_k=0}^{N_k-1}\phi_{nk}(z_i)\phi_{nk}(z_j) = \delta_{i,j}S_k \qquad (14)$$

By inserting the above expansion (12) into the TDSE, we obtain the following set of differential equations for the center of the trajectory $r_k(t)$, the momentum $p_k(t)$, the width $A_k(t)$, and the phase $\gamma_k(t)$:

$$\dot{\mathbf{r}}_k(t) = p_k(t)/m_k \qquad (15)$$

$$\dot{p}_k(t) = -V'_{eff,k} \qquad (16)$$

$$\dot{A}_k(t) = -\frac{2}{m_k}A_k(t)^2 - \frac{1}{2}V''_{eff,k} \qquad (17)$$

$$\dot{\gamma}_k(t) = \frac{p_k(t)^2}{m_k} - i\hbar\frac{\mathrm{Im}\,A_k(t)}{m_k} \qquad (18)$$

where $V'_{eff,k}$ and $V''_{eff,k}$ are effective forces which can be derived on general grounds using the Dirac−Frenkel variational principle.[1,2] However, because the solution of the problem is independent of the forces (only the convergence pattern is affected), we can choose to use the leading terms of these forces, which (see ref 2) are the classical forces. Thus, for the first derivative, we use $V'_{eff,k} = (\partial/\partial\mathbf{r}_k)V_{eff}$ where

$$\frac{\partial V}{\partial r_k} = \frac{\partial V}{\partial x_k}\frac{x_k}{r_k} + \frac{\partial V}{\partial y_k}\frac{y_k}{r_k} + \frac{\partial V}{\partial z_k}\frac{z_k}{r_k} \qquad (19)$$

can easily be obtained because the derivatives $\partial V/\partial x_k$, etc., are used in the classical equations of motion. Equations 15 and 16 show that the center of the packet moves as a classical trajectory. If in addition the second derivative is taken as $V''_{eff,k} = (\partial^2/\partial r_k^2)$-$V_{eff}$, not only do the grid point positions vary with time, as

mentioned before, but also the grid spacings, being a function of $A_k(t)$. In some cases, the equations of motion can lead to large values of Im $A_k(t)$. Thus, to prevent the grid points from collapsing in a very narrow region, an approach where Im $A_k(t)$ is constant can be introduced. This fixed-width treatment is achieved by setting

$$V''_{\mathrm{eff},k} = 4\ \mathrm{Im}\ A_k(t)^2/m_k \tag{20}$$

instead of the second derivative of the potential.

Together with the 18 classical equations of motion in Jacobi coordinates, the following set of equations for the expansion coefficient is obtained:[1,2]

$$i\hbar 3\dot{a}_{n_1n_2} = \sum_{m_1m_2} a_{m_1m_2} W_{n_1n_2;m_1m_2} + a_{m_1m_2}\left[(2n_1+1)\frac{\hbar\ \mathrm{Im}\ A_1}{m_1} + (2n_2+1)\frac{\hbar\ \mathrm{Im}\ A_2}{m_2}\right]\delta_{n_1m_1}\delta_{n_2m_2} \tag{21}$$

where

$$W_{ij,i'j'} = \langle\phi_i\phi_j|V(\mathrm{r}_{1_i},\mathrm{r}_{2_j}) - V'_{\mathrm{eff},1}(\mathrm{r}_{1i} - \mathrm{r}_1(t)) - V'_{\mathrm{eff},2}(\mathrm{r}_{2j} - \mathrm{r}_2(t)) + -\frac{1}{2}V''_{\mathrm{eff},1}(\mathrm{r}_{1i} - \mathrm{r}_1(t))^2 - \frac{1}{2}V''_{\mathrm{eff},2}(\mathrm{r}_{2j} - \mathrm{r}_2(t))^2|\phi_{i'}\phi_{j'}\rangle \tag{22}$$

If we now use

$$d_{ij} = c_{ij}\sqrt{S_1S_2} \tag{23}$$

and put eq 12 into eq 21, we get the coupled equations in the DVR framework as

$$i\hbar\dot{d}_{ij} = W_{ij;i'j'}d_{ij}\delta_{ii'}\delta_{jj'} + \frac{\hbar\ \mathrm{Im}\ A_1}{m_1}\sum_{k=1}^{N_1} d_{kj}T^{(1)}_{ik}\delta_{jj'} + \frac{\hbar\ \mathrm{Im}\ A_2}{m_2}\sum_{k=1}^{N_2} d_{ik}T^{(2)}_{jk}\delta_{ii'} \tag{24}$$

where

$$T^{(1)}_{ik} = \frac{1}{S_1}\sum_{n_1=0}^{N_2-1}\phi_{n_1}(z_i)(2n_1+1)\phi_{n_1}(z_k) \tag{25}$$

$$T^{(2)}_{kj} = \frac{1}{S_2}\sum_{n_2=0}^{N_2-1}\phi_{n_2}(z_j)(2n_2+1)\phi_{n_2}(z_k) \tag{26}$$

Thus the potential matrix is diagonal and the kinetic energy terms are block diagonal, so that the matrix which couples the grid points is sparse, which makes it particularly convenient to use the Lanczos method to propagate eq 24.

In this section, we have given the quantum mechanical equations of motion (24), which are consistent to solve if one wants to introduce quantum corrections to the classical dynamical ones. Once these equations have been obtained, we can solve the classical dynamics using for instance Jacobi coordinates. All we need to do is to calculate the classical forces $\partial V/\partial \mathrm{r}_i$ and use these forces for the effective ones $V'_{\mathrm{eff},i}$ in the definition of the potential matrix elements W. So the recipe is the following:

(1) Set up the classical equations of motion in the coordinate system of choice.

(2) Decide upon the degrees of freedom which should have more than one grid point. This choice defines the quantum degrees of freedom.

(3) Calculate the classical Newton force for the quantum degrees of freedom.

(4) Use these forces together with the fixed width forces $V''_{\mathrm{eff},i}$ to obtain W at the DVR points.

(5) Propagate the classical and quantum equations of motion.

3. Initialization and Analysis

The initialization of the classical variables was carried out as in ref 9; that is, random values of impact parameter (orbital angular momentum), rotational angular momenta, corresponding angles, as well as the orientation of the two molecules are chosen. The initial distance $\mathbf{R}(t_0)$ was taken to be sufficiently large that the interaction potential becomes negligible.

Concerning the initialization of the quantum wave packet, the initial wave function is taken as the product of two Morse oscillator wave functions representing the vibrations of the two molecules:

$$\psi(\mathrm{r}_1, \mathrm{r}_2, t=0) = \Psi^{\mathrm{Morse}}_{\upsilon_1}(\mathrm{r}_1)\Psi^{\mathrm{Morse}}_{\upsilon_2}(\mathrm{r}_2) \tag{27}$$

To obtain the initial expansion coefficients $d_{ij}(t_0)$, we need to project the initial wave function (27) onto the Gauss-Hermite functions:

$$d_{ij}(t_0) = \left(\frac{\hbar}{2\ \mathrm{Im}\ A_1(t_0)}\right)^{1/4}\left(\frac{\hbar}{2\ \mathrm{Im}\ A_2(t_0)}\right)^{1/4}\exp\left(\frac{i}{\hbar}[p_{\mathbf{r}_1}(t_0)(\mathrm{r}_{1_i} - \mathrm{r}_1(t_0)) + Re\ A_1(t_0)(\mathrm{r}_{1_i} - \mathrm{r}_1(t_0))^2]\right)\exp\left(\frac{i}{\hbar}[p_{\mathbf{r}_2}(t_0)(\mathrm{r}_{2_j} - \mathrm{r}_2(t_0)) + Re\ A_2(t_0)(\mathrm{r}_{2_j} - \mathrm{r}_2(t_0))^2]\right)\frac{1}{\sqrt{S_1S_2}}\Psi^{\mathrm{Morse}}_{\upsilon_1}(\mathrm{r}_{1i})\Psi^{\mathrm{Morse}}_{\upsilon_2}(\mathrm{r}_{2j}) \tag{28}$$

The dynamical evolution of the system in time is thus studied by simultaneously propagating the equations of motion for classical variables, integrated together with the differential equation 24 for the d_{ij}'s. In practice, for each time step Δt, the equations of the classical variables have been propagated with a predictor-corrector method, whereas for eq 24 a Lanczos procedure has been used. The accuracy of the integration procedure can be verified by checking the conservation of the norm of the wave function, of the total energy, and of the total angular momentum.

Each trajectory obtained through the dynamical propagation of the system can be nonreactive or reactive or, unlike pure classical trajectory methods, only part of the wave packet can react. Thus, we can obtain information on probabilities for the reactive event or for inelastic scattering. As a matter of fact, as shown in refs 5 and 6, $|d_{ij}|^2$ represents the probability of being at the grid point i in r_1 and j in r_2. To have the reaction probability $P(t)$ then, it is sufficient to sum over those grid points for which $\mathrm{r}_2 \geq \mathrm{r}_2^*$, i.e., where the OH bond can be considered as broken:

$$P(t) = \sum_i\sum_{j\geq j^*}|d_{ij}(t)|^2 \tag{29}$$

Within this approach, it is not necessary to insert an absorbing potential as we do in ordinary grid methods (see ref 9), provided

that the number of grid points employed is sufficient to follow the dynamics.

Note that as the grid moves the grid point j^* corresponding to r_2^* is not fixed but moves in time. As for a mixed quantum classical method, for each trajectory, the probability $P(t)$ is not necessary an integer, as is the case in classical mechanics where the only two possibilities are that of a non reactive event ($P(t) = 0$) or of a completely reactive collision ($P(t) = 1$). Once the probability of reaction is defined, we can obtain the reaction cross section and the rate constant. The rate constant is defined as[28]

$$k(T) = \sqrt{8k_B T/\pi\mu}(T_0/T)^3 \int_0^\infty \mathrm{d}(\beta E) \exp(-(E - E_{n_1 n_2})/k_B T)\,\langle\sigma_R\rangle \quad (30)$$

Here E is the total energy, $E - E_{n_1 n_2} = E_{cl}$ is the sum of kinetic, rotational and vibrational energy of both molecules, and T_0 is an arbitrary reference temperature. $\langle\sigma_R\rangle$ is the so-called average cross section for the reaction, defined by

$$\langle\sigma_R\rangle = \frac{\pi\hbar^6}{8\mu I_1 I_2 (k_B T_0)^3} \sum_{j_1}^{j_1^{max}} \sum_{j_2}^{j_2^{max}} \sum_{l=0}^{l_{max}} (2j_1 + 1)(2j_2 + 1)(2l + 1) P_d \quad (31)$$

This sum is evaluated using a Monte Carlo sampling technique. The initial rotational angular momenta, orbital angular momentum, and orientation of the diatomic molecules in space are chosen randomly. The reaction probability for a given trajectory is given as P_d and determined by eq 29 for $t \rightarrow \infty$. The average cross section $\langle\sigma_R\rangle$ (not to be confused with the reaction cross section!) has been calculated at a number of energies E_{cl}, the sum of the kinetic and rotational energies of both molecules (see below).

Calculations

The total reaction cross sections were computed at 15 distinct values of the energy E_{cl} in the range of 2.5−2000 kJ/mol. The cross sections were estimated using logarithmic interpolation between the 15 energies and extrapolation to energies below 2.5 kJ/mol when computing the rate-constant using eq 30. Because of formation of collision complexes, the cross sections are expensive to evaluate in the low energy region. The cross sections $\langle\sigma_R\rangle$ were evaluated using the "2D quantum-classical" method as well as the TDGH-DVR method. The results of purely classical trajectories are also reported for comparison. The potential energy surface for the HO−CO system was that of Schatz et al.[12] The grid size used for the 2D quantum-classical method was (64:128); this was reduced to (21:129) for the TDGH-DVR method to reduce computation time. However, this did not affect convergence. The two methods are different in several respects. In the 2D quantum-classical method, a fixed grid with absorbing boundary conditions was used. In the TDGH-DVR method, the grid follows the trajectory in space. The parameters used in the calculations are given in Table 1.

We have in Figure 1 shown the wave packet evolve in time. We notice that part of the wave packet stays in the reactive region (large value of $\mathbf{r}_2$) even when the collision trajectory is nonreactive. The reason for this is that with 129 grid points around $\mathbf{r}_2(t)$ we cover the reactive region, even if the trajectory is nonreactive.

The average cross sections at some of the lower energies are given in Table 2.

TABLE 1: Parameters Used in the Calculations[a]

parameter	value: 2D quantum-classical	value: TDGH-DVR
b_{max}/Å	3	3
D_{OH}(100 kJ/mol)	4.4586	4.4586
D_{CO}(100 kJ/mol)	10.8314	10.8314
β_{OH}/Å^{-1}	2.2962	2.2962
β_{CO}/Å^{-1}	2.2996	2.2996
$\mathbf{r}_1$ (CO)/Å	1.1283	1.1283
$\mathbf{r}_2$ (OH)/Å	0.9696	0.9696
$\mathbf{r}_{proj}$/Å	2.9	2.9
N_{r_1}	64	21
N_{r_2}	128	129
($r_{1_{min}}$, $r_{1_{max}}$,Δr_1)/Å	0, 2, 0.031	0.686, 1.5706, 0.042
($r_{2_{min}}$, $r_{2_{max}}$,Δr_2)/Å	0, 5, 0.039	−2.09, 4.029, 0.047
R_0/Å	7.0	7.0

[a] Both the CO and the OH molecule were initially in the vibrational ground state. N_{r_1} and N_{r_2} are the number of grid points along $\mathbf{r}_1$ and $\mathbf{r}_1$. R_0 is the initial separation of the centers of mass.

For energies below 200 kJ/mol, 1000 trajectories were evaluated to ensure convergence of the average reaction cross sections to less than 10%; however, at higher energies, 200 trajectories were sufficient. Energies greater than 700 kJ/mol required the maximum impact parameter, b_{max}, to be augmented from 3 to 4 Å.

The initial separation of the centers of mass of the two reactants was set to 7 Å, at which distance the interaction potential is negligible. We notice that the average cross sections obtained with the 2D quantum-classical method are much larger (at low energies) when compared to the numbers obtained with the TDGH-DVR method. The classical trajectories underestimate the cross sections at 5 kJ/mol, because of the lack of tunneling possibility in this theory.

The lifetime, τ, of the HOCO radical complex was also estimated from the duration of the collision t and the initial kinetic energy of each trajectory:

$$\tau = t - t_{coll} = t - \frac{2R_0}{\upsilon_R} \quad (32)$$

where R_0 is the initial separation of the reacting species and υ_R is the velocity along the center of mass coordinate. t is the duration of the trajectory, and t_{coll} is the time required by the reactants to travel the distance $2R_0$ without the interaction potential. The difference is the duration of time that the reactants exist as a complex. Trajectories for which $t_{coll} \geq t$ were nonreactive as no complex was formed. The average lifetimes at $E_{cl} = 5$ and $E = 10$ kJ/mol were found to be 2942 and 1707 fs, respectively, confirming that a long-lived complex is formed at low energies during the reaction. These numbers are in good agreement with earlier estimates, which at somewhat higher energies are around and less than 1 ps.[23,24]

Experimentally, the rate of reaction of carbon monoxide with the hydroxyl radical has been studied extensively at and around 298 K.[25,29] The low-pressure limit rate constant for this reaction is 1.5×10^{-13} cm^{-3} s^{-1} at 298 K, and several studies[25] have concluded that it is practically constant in the temperature range 200−400 K. This non-Arrhenius temperature dependence is characteristic of complex-forming bimolecular reactions. This agrees well with the calculations presented in this work; the new TDGH-DVR method predicts a rate constant at 298 K of 1.49×10^{-13} cm^{-3} s^{-1}with a standard deviation of ($\sigma = 0.25 \times 10^{-13}$). Our calculated rate constant is also nearly invariant in the range 100−350 K, see Figure 2. At low temperatures,

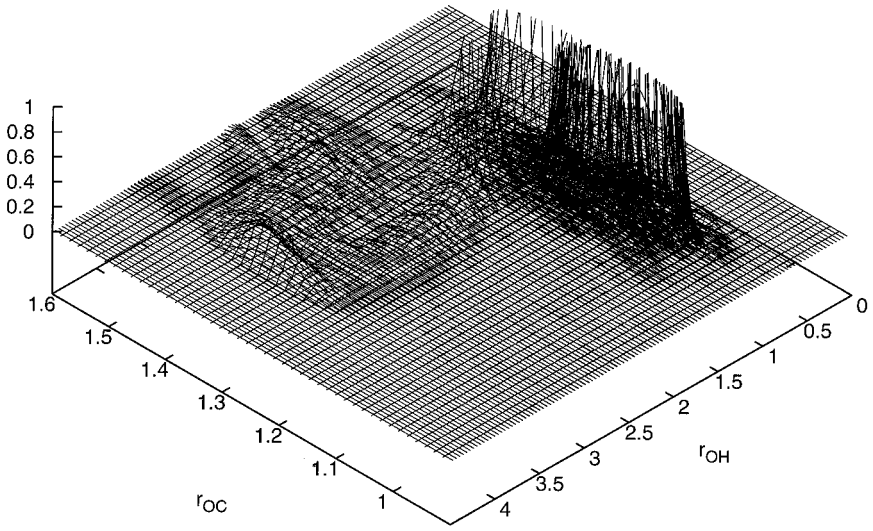

Figure 1. Wave packet which is initially a product of two Morse oscillator functions in the OC and OH bond located around the equilibrium distances. At later times, the packet moves on the DVR grid, and the figure shows that the amplitude is building up at large values of the OH bond, indicating that a chemical reaction has taken place. The reaction probability is obtained as the grid summed total squared amplitude for $\mathbf{r}_{OH}$ bond lengths exceeding a 2.9 Å.

TABLE 2: Total Average Reaction Cross Sections $\langle\sigma_R\rangle$, Å² eq 31, Calculated for the Classical and Quantum-Classical Trajectories[a]

E_{cl} (100 kJ/mol)	σ, classical	σ, 2D quantum-classical	σ, TDGH-DVR
0.05	$2.5 \times 10^{-5}(\pm 2.5 \times 10^{-6})$	$0.3\ (\pm 3 \times 10^{-2})$	$2 \times 10^{-2}\ (\pm 2 \times 10^{-3})$
0.1	0.55 (±0.03)	1.4 (±0.018)	0.25 (±0.02)
0.2	5 (±0.3)	14 (±1)	2 (±0.1)
0.3	4 (±0.2)	44 (±3)	8 (±0.2)
0.4	10 (±1.2)	88 (±7)	31 (±3)
0.5	82 (±5)	164 (±6)	268 (±13)
1	2224 (±170)	2371 (±130)	3450 (±120)
2	60 000 (±2800)	65 000 (±3520)	60 700 (±2640)

[a] Errors correspond to one mean standard deviation.

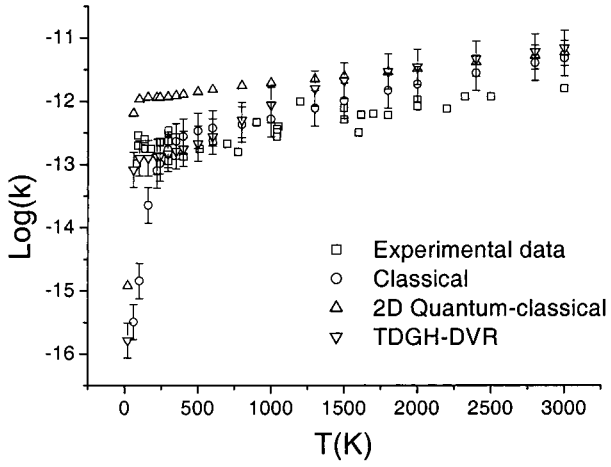

Figure 2. Rate constant, k, for the reaction CO + OH as a function of temperature. The rates calculated using a 2D quantum-classical method and the new TDGH-DVR method are compared to a purely classical method and experimental data. The experimental data are taken from refs 14, 15, 25, 29, and 30

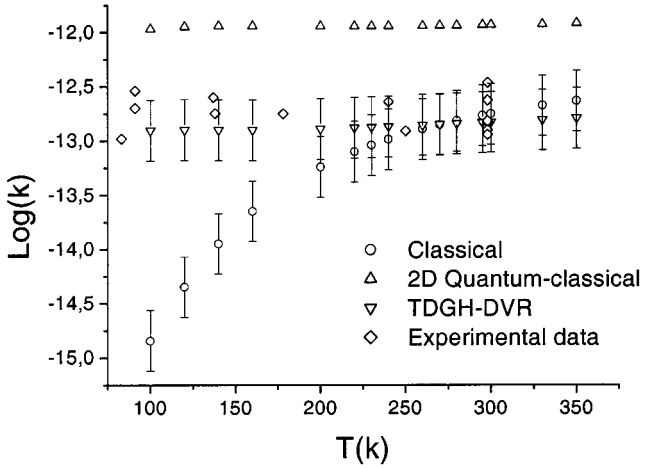

Figure 3. Rate constant of the reaction of CO with OH in the temperature range 100−350 K. The experimental data are taken from refs 14, 15, 25, 29, and 30.

there are relatively few available experimental data. One study[30] reports rate constants for the reaction from 296 K down to near liquid nitrogen temperature at 80 K. These values are indicated in Figure 3 at 178, 138, and 80 K and are in good agreement with the TDGH-DVR calculations. Another study by Fulle et al.[14] reports rate constants at 137 and 91 K that are also in good agreement with the TDGH-DVR (see Figure 2). At higher temperatures, the difference between the quantum-classical and the quasiclassical rates become small.

A recent study by Golden et al.[14] sums up the available high-temperature rate data for the reaction (400−3000 K), these values follow the same trend as our calculated rate data even if they are generally lower. At high temperatures (combustion conditions), experimental error is relatively larger[14] than at intermediate temperatures, as the kinetic studies usually employ

indirect methods and often probe the reverse reaction, $CO_2 + H \rightarrow CO + OH$.

Acknowledgment. Professor George Schatz is acknowledged for providing us with the latest surface on HO + CO.

References and Notes

(1) Billing, G. D. *J. Chem. Phys.* **1997**, *107*, 4286.
(2) Billing, G. D. *J. Chem. Phys.* **1999**, *110*, 5526.
(3) Billing, G. D.; Adhikari, S. *Chem. Phys. Lett.* **1999**, *309*, 249.
(4) Adhikari, S.; Billing, G. D. *J. Chem. Phys.* **2000**, *113*, 1409.
(5) Billing, G. D.; Adhikari, S. *Chem. Phys. Lett.* **2000**, *321*, 197.
(6) Billing, G. D. *Chem. Phys.* **2001**, *264*, 71; *J. Chem. Phys.* **2001**, *114*, 6641.
(7) Billing, G. D. *J. Phys. Chem.* **2001**, *105*, 2340.
(8) Billing, G. D. *Chem. Phys. Lett.* **2001**, *339*, 237.
(9) Coletti, C.; Billing, G. D. *J. Chem. Phys.* **2001**, *113*, 11101.
(10) Mozurkewich, M.; Lamb, J. J.; Benson, S. W. *J. Phys. Chem.* **1984**, *88*, 6435.
(11) Clary, D. C.; Schatz, G. C. *J. Chem. Phys.* **1993**, *99*, 4579.
(12) Bradley, K. S.; Schatz, G. C. *J. Chem. Phys.* **1997**, *106*, 8464.
(13) Duncan, T. V.; Miller, C. E. *J. Chem. Phys.* **2000**, *113*, 5138.
(14) Golden, D. M.; Smith, G. P.; McEwan, A. B.; Yu, C.-L.; Eiteneer, B.; Frenklach, M.; Vaghjiani, G. L.; Ravishankara, A. R.; Tully, F. P. *J. Phys. Chem. A* **1998**, *102*, 8598.
(15) Frost, M. J.; Sharkey, P.; Smith, I. W. M. *Faraday Discuss. Chem. Soc.* **1991**, *91*, 305.
(16) Fulle, D.; Hartman, H. F.; Hippler, H.; Troe, J. *J. Chem. Phys.* **1996**, *105*, 983.
(17) Stevens, C. M.; Kaplan, L.; Gorse, R.; Durkee, S.; Compton, M.; Cohen, S.; Bielling, K. *Int. J. Chem. Kinet.* **1980**, *12*, 935.
(18) Brunning, J.; Derbyshire, D. W.; Smith, I. W. M.; Williams, M. D. *J. Chem. Soc., Faraday Trans. 2* **1988**, *84*, 105.
(19) Röckmann, T.; Brenninkmeijer, C. A. M.; Saueressig, G.; Bergamaschi, P.; Crowley, J. N.; Fischer, H.; Crutzen, P. J. *Science* **1998**, *281*, 544.
(20) Weston, R. E. *Chem. Rev.* **1999**, *99*, 2115.
(21) Lester, M. I.; Pond, B. V.; Anderson, D. T.; Harding, L. B.; Wagner, A. F. *J. Chem. Phys.* **2000**, *113*, 9889.
(22) Zhang, D. H.; Zhang, J. Z. H. *J. Chem. Phys.* **1995**, *103*, 6512. Goldfield, E. M.; Gray, S. K.; Schatz, G. C. *J. Chem. Phys.* **1995**, *102*, 8807.
(23) Balakrishnan, N.; Billing, G. D. *J. Chem. Phys.* **1995**, *104*, 4005.
(24) Clary, D. C.; Schatz, G. C. *J. Chem. Phys.* **1993**, *99*, 4578.
(25) DeMore, W. B.; Sander, S. P.; Golden, D. M.; Hampson, R. F.; Kurylo, M. J.; Howard, C. J.; Ravishankara, A. R.; Kolb, C. E.; Molina, M. J. *Chemical Kinetics and Photochemical Data for Use in Stratospheric Modeling, Evaluation Number 12*; JPL Publication 97-4; Jet Propulsion Laboratory, California Institute of Technology: Pasadena, CA, 1997.
(26) Billing, G. D.; Mikkelsen, K. V. *Introduction to Molecular Dynamics and Chemical Kinetics*; Wiley: New York, 1997.
(27) Balakrishnan, N.; Billing, G. D. *J. Chem. Phys.* **1994**, *101*, 2785.
(28) Billing, G. D. *Comput. Phys. Comm.* **1984**, *1*, 237.
(29) *NIST Chemical Kinetics Database*, 17-2Q98; NIST Standard Reference Data: Gaithersburg, MD, 1998.
(30) Frost, M. J.; et al. *J. Phys. Chem.* **1993**, *97*, 12254−12259.